The effect of the rheological column on the structural style in progressive arcs: ductile and brittle-ductile analogue models

El efecto de la columna reológica sobre el estilo estructural en arcos progresivos: modelos analógicos dúctiles y frágil-dúctiles

Alejandro Jiménez-Bonilla, M. Trinidad Soriano and Ana Crespo Blanc

Departamento de Geodinámica-Instituto Andaluz Ciencias de la Tierra, Universidad de Granada-CSIC. Universidad de Granada, 18071. Granada, España.

ABSTRACT

Analogue models have been performed to simulate a progressive arc indenting in a parallelepiped composed only of silicone and of silicone and a layer of sand of progressively increasing thickness. The experiments permit to study the ductile deformation within the silicone and the influence of the sand thickness on the development of structures. To do so, we used an indenter that diminished its curvature ratio while its protrusion degree increased with progressive deformation. In all models, strain was partitioned between arc-perpendicular shortening and arc-parallel stretching. In silicone models, the deformation was homogeneous, while even when a very thin sand layer was sieved on top, heterogeneous deformation was observed, and folds, thrusts, strike-slip and normal faults formed. With increasing sand layer thickness, folds wavelength increases and blocks capped by sand individualize and rotate clockwise and counterclockwise in the left and right arc limbs, respectively. With progressive deformation, some of these structures evidence a change in the kinematic regime because of rotations around a vertical axis.

Key-words: *analogue models, progressive arcs, silicone-sand parallelepiped, strain partitioning*

RESUMEN

Se han hecho modelos analógicos con un backstop que simula un arco progresivo deformando un paralelepípedo compuesto sólo por silicona y con una capa de arena cuyo espesor se incrementó progresivamente. Esto permite estudiar la deformación dúctil en la silicona y la influencia del espesor de arena en el desarrollo de estructuras. Para ello, usamos un indenter que disminuyó su radio de curvatura mientras su grado de protrusión se incrementó con la deformación progresiva. En todos los modelos se observó un reparto de la deformación entre acortamiento perpendicular y estiramiento paralelo al arco. En los modelos con silicona, la deformación fue homogénea mientras que al poner una fina capa de arena sobre ella, se observó deformación heterogénea, y se formaron pliegues, cabalgamientos, fallas de salto en dirección y normales. A medida que se incrementa el espesor de arena, la longitud de onda de los pliegues aumenta y se individualizan bloques que rotan en el sentido horario y antihorario en el flanco izquierdo y derecho, respectivamente. Con la deformación progresiva, algunas estructuras evidencian un cambio de régimen cinemático por rotaciones en el eje vertical.

Palabras clave: *modelos analógicos, arcos progresivos, paralelepípedo de silicona y arena, reparto de la deformación.*

Geogaceta, 64 (2018), 19-22
ISSN (versión impresa): 0213-683X
ISSN (Internet): 2173-6545

Recepción: 31 de enero de 2018
Revisión: 9 de abril de 2018
Aceptación: 25 de abril de 2018

Introduction

Recent analogue models permit to simulate progressive arcs with an indenter that lengthens and protrudes in map view while the experiment progresses (Jiménez-Bonilla *et al.*, 2016; Crespo-Blanc *et al.* 2017). As this indenter was rigid enough, it acted as a backstop deforming an initial parallelepiped composed of silicone and sand. These experiments were made to reproduce in laboratory the brittle-ductile deformation of the external fold-and-thrust belts in Mediterranean Arcs (*e.g.*, Crespo-Blanc *et al.*, 2017). The models resulted in highly segmented, non-cylindrical arcuate deformed wedges affected by thrust, folds, strike-slip and normal faults that accommodated outward-radial tectonic transport and vertical axis rotations (Jiménez-Bonilla *et al.*, 2016). In those experiments, the thickness of the brittle layer: the sand, which simulates sedimentary rocks, was constant (1.5 cm) while the thickness of the silicone layer, which simulates the ductile flow of evaporites in natural cases, varied from 1 to 2 cm. However, we found to the need to further investigate the consequences of variation of the sand layer thickness on strain partitioning of arcuate fold-and-thrust belts, and also to check the viscous deformation in the silicone without any overlaid sand in front of such indenter. With these premises, in this research we used the same backstop as Jiménez-Bonilla *et al.* (2016) to carry out experiments with a bottom layer of silicone overlaid or not by sand, and whose thickness progressively increased in order to: (1) study the ductile deformation within the silicone, (2) investigate the influence of the increase in sand thickness on type, distribution and kinematics of the structures that formed in the progressive arc models, and (3) compare with previous brittle-ductile models of progressive arcs with both

different initial geometry and thicknesses of the initial parallelepiped (Jiménez-Bonilla *et al.*, 2016).

Model Set Up

The experiments were run in the Analogue Modeling Laboratory of the Geodynamics Department – Andalusian Earth Science Institute in Granada. The size of the initial parallelepiped is 56 cm width x 53 cm long. It is floored by a drafting film sheet and confined by wood strips and a plastic strip in one of the sides (Fig. 1). A screw is attached to the plastic strip, thus this side acted as progressive arc backstop with the screw pushing at a velocity of 1.07 cm/hour. A 3 cm-side reference grid was sieved on top of the initial parallelepiped when a layer of sand overlaid the silicone. For the experiments with silicone only, we draw this grid with an indelible marker. The indenter diminished its curvature ratio while its protrusion grade increased with progressive deformation (Fig. 1, see also Jiménez-Bonilla *et al.*, 2016).

Six experiments were carried out: Models 1 and 2 were made up of a silicone layer, 0.4 cm and 1 cm thick, respectively. In Models 3 to 6, a sand layer of 0.1, 0.3, 0.6 and 1 cm thick, respectively, was sieved on top of a 0.5 cm thick silicone layer.

The amount of displacement of the plastic strip at the apex varies between 26 and 38.2 cm. The progressive deformation was recorded by time lapse photography in plan view. Additionally, oblique pictures were taken after experiments. Sand was carefully removed in two experiments (Models 3 and 4) and some cross-sections were made in Model 6. The physical properties of the analogue materials and the scaling are fully described in Crespo-Blanc (2008) and Jiménez-Bonilla *et al.* (2016).

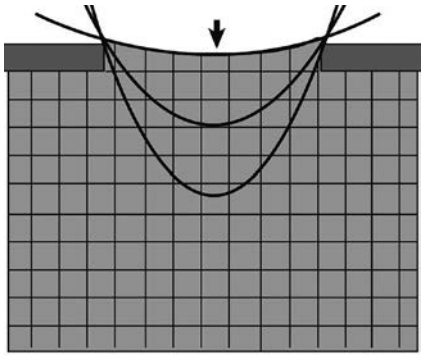

Fig. 1.- Simplified sketch of the experimental apparatus in plan view. Observe the progressive arc geometry while experiment proceeds (from t0 to t2). Vertical markers are parallel to the apex displacement.

Fig. 1.- Esquema simplificado en planta de la mesa de trabajo. Obsérvese la geometría progresiva del arco cuando progresa el experimento (de t0 a t2). Los marcadores verticales son paralelos al desplazamiento en el apex

Results

Models 1 and 2 (0.4 and 1 cm silicone thickness, respectively)

The progressive and finite deformation depicted by the reference grid in Models 1 and 2 is nearly identical. The finite deformation is illustrated for Model 2 in figure 2A. At scale of the grid square, the deformation can be considered the homogeneous. Each square is deformed by mostly simple shear in the lateral and internal parts of the Model or mostly pure shear in its most frontal part. As a whole, the line drawing of the final stage shows an accommodation of the grid to the arcuate backstop geometry, accompanied by radial, arc-perpendicular shortening and by arc-parallel stretching. On the surface of the model, the grid markers show that these types of strain are accommodated by millimetric-spaced folds with sharp hinges and linear limbs, and stretching of the markers, respectively, which means that the deformation is not perfectly homogeneous (Fig. 2B).

Due to progressive deformation and associated vertical-axis rotations at the arc limbs, the strain that affected the vertical markers (that is, parallel to the apex displacement) shortened at the first stages, but can vary later from shortening to stretching. Accordingly, folds can be stretched (Fig. 2B).

The squares of the reference grid deformed into rhombs at both arc limbs. It implies clockwise rotations of the horizontal markers and counterclockwise of the vertical ones in the left arc limb, and the opposite senses in the right arc limb (Fig. 2). The distance from the indenting backstop to the first grid marker of the internal part of the model increased progressively (twice its original length at the end of the experiments), which indicates silicone flow towards this part of the model during the experiments.

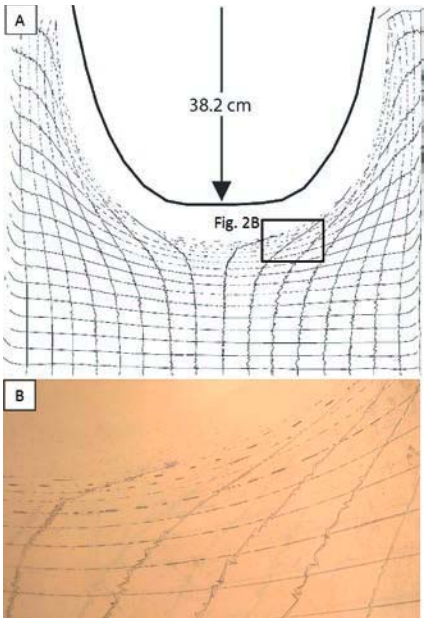

Fig. 2.- A. Line drawing of the markers on top of the silicone of Model 2. B. Detail of the central right part of the arc with kink folds type, stretched markers and stretched folds.

Fig. 2.- A. Dibujo de los marcadores en la planta de la silicona del Modelo 2. B. Detalle de la parte central derecha del arco con pliegues kinks, marcadores estirados y pliegues estirados

Models 3 to 6 (0.1, 0.3, 0.6 and 1.0 cm of sand, respectively)

The presence of a brittle sand layer over the viscous silicone causes deformation to be heterogeneously distributed into discrete structures such as thrusts, folds and normal or strike-slip faults. In figure 3, the line drawings of various stages of the progressive deformation of three representative experiments can be observed. All of these experiments resulted in curved fold-and-thrust belts, in which shortening along the transport direction was accommodated by thrusts, backthrusts and folds while arc-parallel stretching was accommodated by normal and conjugate strike-slip faults (Figs. 3 and 4A).

The first structures to nucleate were strike-slip faults that crossed the Models oblique to the apex movement. Almost simultaneously, foreland verging thrusts and folds developed (Fig. 3). In Model 6 (Fig. 3C), a strike-slip fault parallel to the apex movement formed and quickly evolved into a transtensional fault zone. When deformation proceeded new thrusts and folds formed in the apical part and the wedge widened. Meanwhile, conju-

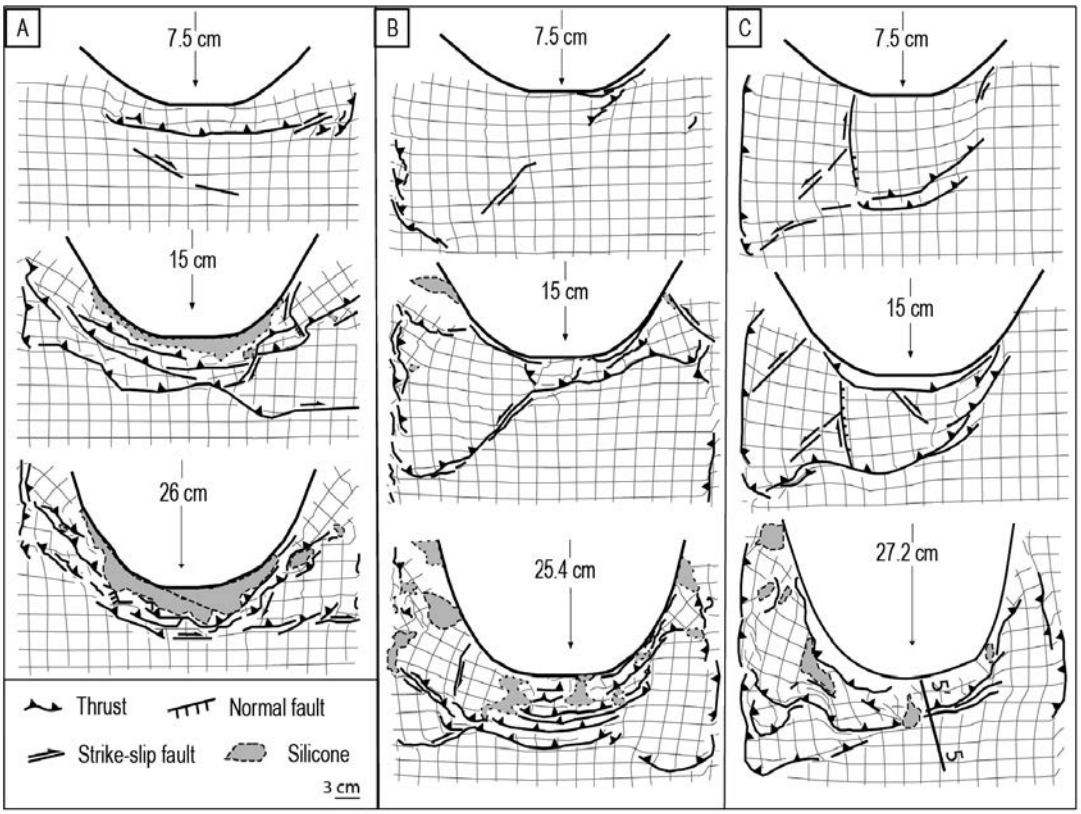

Fig. 3.- A), B) and C) Line drawings showing the deformation sequence in three deformational stages (indicated as centimeters of arc apex displacement) of Models 3, 5 and 6, respectively. Sand layer of 0.1, 0.6 and 1.0 cm, respectively.

Fig. 3.- A), B) y C) Dibujos mostrando la secuencia de deformación en tres estadios de deformación (indicados en centímetros del desplazamiento del ápex del arco) de los Modelos 3, 5 y 6, respectivamente. Capa de arena de 0.1, 0.6 y 1.0, respectivamente

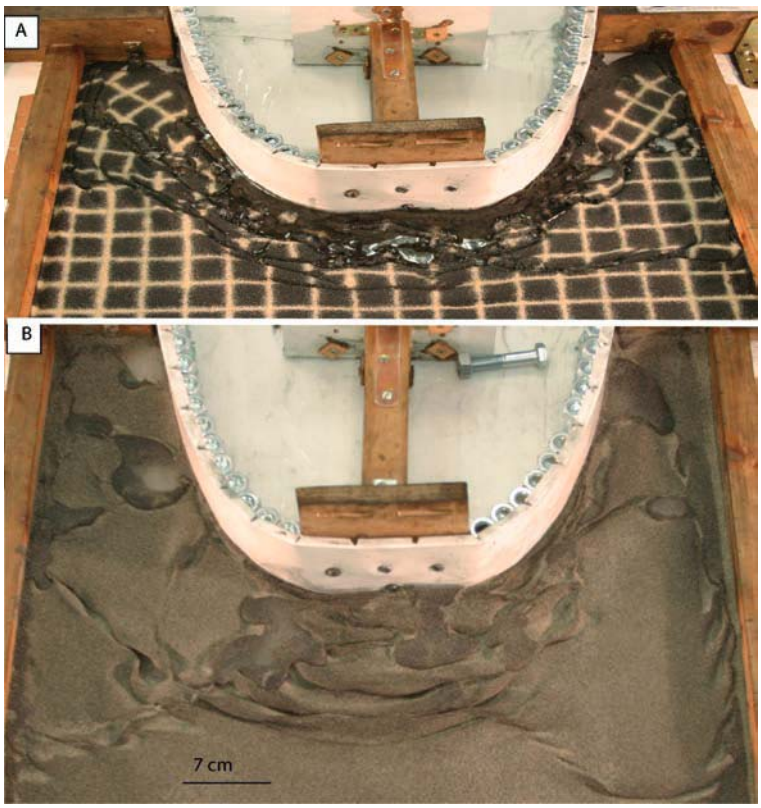

Fig. 4.- A) Oblique picture of Model 3 final stage. B) Silicone topography of Model 5. See color figure in the web.

Fig. 4.- A) Fotografía oblicua del estadio final del Modelo 3. B) Topografía de la silicona del Modelo 5. Ver figura en color en la web.

gate strike-slip faults developed in the lateral parts. Additionally, some normal faults nucleated perpendicular to the thrusts. All these structures individualized blocks that rotated progressively up to 40° clockwise and counterclockwise in the left and right arc limbs, respectively (Fig. 3). Exceptionally, one block rotated in the opposite way, due to border effect (lateral parts of Model 6, Fig. 3C). The thrust wavelength increased from *ca.* 0.5 to 10 cm -and consequently, the width of the blocks- as the sand thickness increased from 0.1 to 1.0 cm.

In the last deformation stages, the kinematics along some of the structures varied because of the vertical axis rotations of the structures due to progressive arching and the corresponding variation of strain type along a structure formed in an early stage (*e.g.*, from thrust to strike-slip fault; Fig. 3A).

Finally, the silicone pierced the surface and quickly flowed, covering part of the fold-and-thrust belt. When the sand layer was thinner, this piercing concentrated in the most internal zones of fold-and-thrust belts (Figs. 3 and 4).

A cross-section nearly parallel to the tectonic transport and located at the apical part of experiment with a 1.0 cm thick sand layer (Model 6) shows a complex structure of foreland and hinterland verging thrusts and, in turn, folds overthrusted by other thrust sheets (Fig. 5). All these structures are detached within the silicone, as shown also by the comparison between the silicone topography (Fig. 4B) and the final stage of Model 5 (Fig. 3B).

Discussion

In all six models, ductile and brittle-ductile strain is partitioned between arc-perpendicular shortening and arc-parallel stretching (Figs. 2 to 5). This is similar to previous experiments that used the same indenter of a progressive arc protruding in a silicone-sand parallelepiped (Jiménez-Bonilla *et al.*, 2016; Crespo-Blanc *et al.*, 2017). In the silicone models, the deformation was homogeneous at the grid scale. However, with the presence of a brittle layer over the viscous one, even if it was very thin, deformation was heterogeneous and discrete structures such as folds, thrusts, strike-slip and normal faults formed. The spacing of these structures is higher when the brittle layer thickness increases, due to strength increase of this brittle layer (*e.g.,* Ramsay and Huber, 1987, Costa and Vendeville, 2002; Simpson, 2009).

In figure 6, we superposed Model 1 line drawing to the photograph of Model 3, both models with the same apex displacement. It is a tentative mode to connect the homogeneous deformation within the viscous layer with the heterogeneous deformation that took place in the brittle layer. Although deformation in the silicone overlaid by a thin layer of sand was not likely the same as that registered within single silicone layer, it should be very similar. This superposition demonstrates that the type of deformation in both models is similar. That is, quasi-homogeneous shortening strain in the ductile model corresponds to thrusts in the model with a brittle layer.

Fig. 5.- Cross-section subparallel to the transport direction (Model 6). See location in Fig. 3C. See color figure in the web.

Fig. 5.- Corte subparalelo a la dirección de transporte (Modelo 6). Localización en la Fig. 3C. Ver figura en color en la web.

The deformed grid on top of the silicone is slightly displaced towards a more frontal part with respect to the brittle-ductile model. There is also a progressive correspondence between the silicone outcrops in the internal part of Model 3 and the zone parallel to the backstop where the silicone accumulated in Model 1 after deformation. Accordingly, this could be related to silicone flow from the bottom of the viscous layer when the backstop pushed it from behind, favored by the silicone buoyancy.

Conclusions

1. Silicone models of progressive arcs with a viscous rheology show homogeneous deformation at grid scale. When a sand layer with a brittle behavior is sieved on top of the silicone layer, discrete structures formed.

2. Strain is partitioned between arc-perpendicular shortening, and arc-parallel stretching, with a similar distribution in both ductile and brittle-ductile models.

3. As the brittle layer thickness is increased, the folds wavelength increases and blocks capped by sand formed and rotated clockwise and counterclockwise in the left and right arc limbs, respectively.

Acknowledgements

This study was supported by projects RNM-0451 (Junta de Andalucía) and CGL2013-46368-P. We thank reviewers Elena Druguet and Cristina García for their constructive revisions.

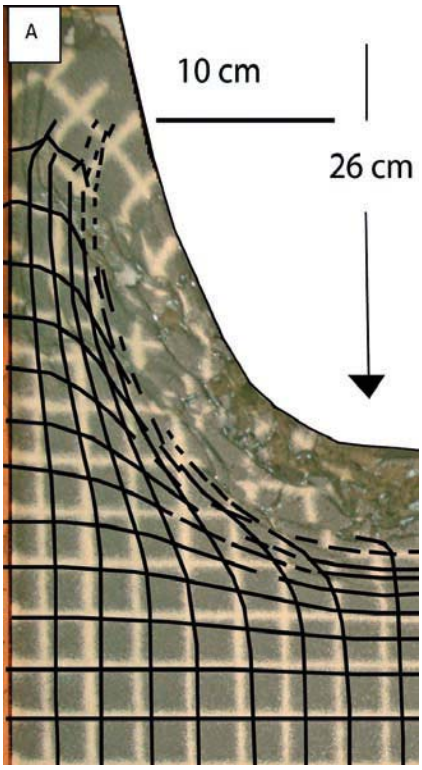

Fig. 6.- Superposition of the left part of Model 3 with the line drawing of Model 1 (same apex displacement). See color figure in the web.

Fig. 6.- Superposición de la parte izquierda del Modelo 3 con el dibujo de Modelo 1 (mismo desplazamiento del ápex). Ver figura en color en la web.

References

Costa, E. and Vendeville, B.C. (2002). *Journal of Structural Geology* 24, 1729–1739.

Crespo-Blanc, A. (2008). *Journal of Structural Geology* 30(1), 65-80.

Crespo-Blanc, A., Jiménez-Bonilla, A., Balanyá, J.C., Expósito, I. and Díaz-Azpiroz, M., (2017). *Geogaceta* 62, 15-18.

Jiménez-Bonilla, A., Crespo-Blanc, A., Balanyá, J.C., Expósito, I. and Díaz-Azpiroz, M. (2016). *Geo-Temas* 16, CD-Rom.

Ramsay, J.G. and Huber, M.I. (1987). *The techniques of modern structural geology – Volume 2: Folds and fractures*. Academic Press, London, 700 p.

Simpson, G.D.H. (2009). *Journal of Structural Geology* 31, 369–381.